Hypovascular Hypointense Nodules on Hepatobiliary Phase Gadoxetic Acid–enhanced MR Images in Patients with Cirrhosis: Potential of DW Imaging in Predicting Progression to Hypervascular HCC[1]

Young Kon Kim, MD, PhD
Won Jae Lee, MD, PhD
Min Jung Park, MD, PhD
Seong Hyun Kim, MD, PhD
Hyunchul Rhim, MD, PhD
Dongil Choi, MD, PhD

Purpose: To investigate the imaging features of hypovascular hypointense nodules on hepatobiliary phase gadoxetic acid–enhanced magnetic resonance (MR) images in patients with cirrhosis that may be associated with progression to hypervascular hepatocellular carcinoma (HCC).

Materials and Methods: The institutional review board approved this retrospective study and waived informed patient consent. This study included 135 patients with a diagnosis of hepatitis B–induced liver cirrhosis and 214 hypovascular hypointense nodules on hepatobiliary phase gadoxetic acid–enhanced MR images. MR images were analyzed with respect to nodule size, degree of hypointensity at hepatobiliary phase (four grades), presence of fat, and signal intensity on T1- and T2-weighted and diffusion-weighted (DW) images. Univariate and multivariate Cox regression analyses were used to identify variables that are associated with developing hypervascular HCC.

Results: On follow-up MR images, 139 nodules (65.0%) had no evidence of HCC (mean follow-up, 522 days) (group 1), but 75 (35.0%) became hypervascular HCC (mean follow-up, 388 days) (group 2). Univariable Cox analysis revealed that the degree of hypointensity on hepatobiliary phase images (P = .044 and .001) and hyperintensity on T2-weighted and DW images (P = .001 and .0001) was significantly related to the development of hypervascular HCC. According to the multivariable Cox analysis, no other variable significantly adjusted the model once hyperintensity at initial DW imaging was already included as an associated variable, (hazard ratio, 7.44; 95% confidence interval: 4.28, 12.94; P = .0001).

Conclusion: Hyperintensity on DW images in hypovascular hypointense nodules on hepatobiliary phase gadoxetic acid–enhanced MR images in patients with cirrhosis is strongly associated with progression to hypervascular HCC.

[1] From the Department of Radiology and Center for Imaging Science, Samsung Medical Center, Sungkyunkwan University School of Medicine, 50 Ilwon-dong, Gangnam-gu, Seoul 135-710, Republic of Korea. Received December 14, 2011; revision requested January 30, 2012; revision received February 28; accepted March 28; final version accepted April 19. **Address correspondence to** W.J.L. (e-mail: *wjlee@skku.edu*).

Most hepatocellular carcinomas (HCCs) develop in patients with underlying chronic hepatitis or cirrhosis via a multistep process of carcinogenesis, ranging from regenerative nodules to classic HCC (1–4). Owing to technical advances in liver imaging and surveillance for those at high risk for developing HCC, we increasingly encounter borderline hepatocellular nodules in the gray area of multistep carcinogenesis. By using only dynamic imaging with extracellular space contrast agents, which rely on highlighting the differences in blood supply, it is difficult to accurately characterize and detect borderline hepatocellular nodules. This is because the differences in angioarchitecture are not remarkable among borderline hepatocellular nodules or between borderline hepatocellular nodules and cirrhotic liver (1–4). Accordingly, both early HCC and dysplastic nodules may appear as isoattenuated (or isointense) nodules or low-attenuating (or hypointense) nodules on contrast material–enhanced computed tomographic (CT) or magnetic resonance (MR) images (3).

Gadolinium ethoxybenzyl diethylenetriamine pentaacetic acid (gadoxetic acid disodium, Primovist; Bayer Healthcare, Berlin, Germany) has recently been widely used as an MR contrast agent for dual imaging, having the characteristics of an extracellular fluid space contrast agent during the early vascular and interstitial phases and of a liver-specific hepatocellular agent during the delayed phase (5–7). In the evaluation of patients suspected of having HCC, the most useful feature of gadoxetic acid is better depiction of HCC as hypointensity on hepatobiliary phase (HBP) images than at equilibrium phase of conventional dynamic images (7–10). When the hypointensity on HBP images is accompanied by arterial hypervascularization, the hypointensity at HBP is confirmative of HCC (7–10). However, benign hepatocellular nodules or early HCCs without sufficient arterial neovascularity can be seen as hypointense only on HBP images and may transform into hypervascular HCC on follow-up imaging studies (10,11). Currently, there are no exact guidelines to differentiate HCC and benign hepatocellular nodules in patients with hypointense nodules seen only on HBP images or to identify nodules at high risk for progression to hypervascular HCC. Since precise histopathologic differentiation between high-grade dysplastic nodules and early HCC is still difficult, it is also challenging to determine the definitive imaging finding of those borderline nodules, even with multi-imaging modalities (12). Thus, unless aggressive diagnostic procedures such as percutaneous biopsy or curative techniques are considered, those lesions must be followed up with imaging and clinical evaluation because they are biologically benign until arterial hypervascularization is shown to develop within the nodules (11,13).

In this context, we conducted this study to investigate the imaging features of hypovascular hypointense nodules on HBP gadoxetic acid–enhanced MR images in patients with cirrhosis that may be associated with progression to hypervascular HCC.

Advances in Knowledge

- In patients with cirrhosis examined with gadoxetic acid, hyperintensity on high-*b*-value (800 sec/mm^2) diffusion-weighted (DW) images is associated with progression of hypovascular hypointense nodules to hypervascular hepatocellular carcinoma (HCC).
- In patients with cirrhosis examined with gadoxetic acid, the mean apparent diffusion coefficient of hypovascular hypointense nodules that progressed to hypervascular HCC was significantly lower than that of stable nodules (1.14 ± 0.12 vs 1.26 ± 0.14; P = .001).

Implication for Patient Care

- DW imaging with gadoxetic acid–enhanced MR imaging is useful for early detection of hypointense nodules in the hepatobiliary phase that are at high risk for progression into hypervascular HCC.

Materials and Methods

Patients

This retrospective study had institutional review board approval, and informed consent was waived. Our institutional database was searched for liver MR imaging examinations conducted in patients with a diagnosis of liver cirrhosis between September 2008 and September 2010 by using the search term *indeterminate* OR *borderline hepatocellular nodule* OR *hypointense nodule on HBP*. This search identified 200 patients. The inclusion criteria were *(a)* patients with hypovascular hypointense nodules on HBP gadoxetic acid–enhanced MR images, *(b)* patients who underwent liver MR imaging that included gadoxetic acid–enhanced imaging and diffusion-weighted (DW) imaging with use of a 3.0-T system, and *(c)* patients who underwent follow-up liver MR imaging because most hypointense nodules seen only on HBP gadoxetic acid–enhanced MR images were not clearly depicted on multi–detector row CT images. Of the 200 patients, 65 were excluded for the following reasons: 41

Published online before print
10.1148/radiol.12112649 **Content code:** GI

Radiology 2012; 265:104–114

Abbreviations:
ADC = apparent diffusion coefficient
CI = confidence interval
DW = diffusion weighted
HBP = hepatobiliary phase
HCC = hepatocellular carcinoma

Author contributions:
Guarantors of integrity of entire study, Y.K.K., W.J.L., M.J.P.; study concepts/study design or data acquisition or data analysis/interpretation, all authors; manuscript drafting or manuscript revision for important intellectual content, all authors; approval of final version of submitted manuscript, all authors; literature research, Y.K.K., W.J.L., D.C.; clinical studies, Y.K.K., W.J.L., M.J.P., S.H.K., H.R.; statistical analysis, Y.K.K.; and manuscript editing, all authors

Potential conflicts of interest are listed at the end of this article.

had no follow-up MR images or were lost to follow-up, 20 had hyperintense borderline nodules on HBP images, and four had too many nodules (>15) to allow a matched analysis. Of the 41 who had no follow-up MR images, six and eight hypointense nodules on HBP images proved to be hypovascular HCCs and cirrhosis-associated benign hepatocellular nodules (five low-grade and three high-grade dysplastic nodules), respectively, based on histopathologic examination findings via surgery. Six HCCs and one high-grade dysplastic nodule were hyperintense on initial DW images. Thus, the remaining 135 patients (96 men and 39 women; age range for men, 37–78 years; mean age, 59 years; age range for women, 55–70 years; mean age, 61 years; age range for all patients, 37–78 years; mean age, 60 years) formed the final study group. All patients had liver cirrhosis associated with only viral hepatitis B. Of these patients, 112 had a history of HCC before performance of the initial MR examination. In eight patients, concomitant single HCC was observed at initial MR imaging. These HCCs were also treated with surgery (n = 50), transarterial chemoembolization (n = 45), and radiofrequency ablation (n = 25).

A total of 214 hypovascular hypointense nodules on HBP gadoxetic acid–enhanced 3.0-T MR images were identified in the 135 patients: 87 patients had one solitary lesion, 31 patients had two lesions, nine patients had three lesions, three patients had four lesions, four patients had five lesions, and one patient had six lesions. Of these, 139 nodules did not show evidence of progression to hypervascular HCC over time at follow-up imaging (group 1) (mean follow-up, 522 days; range, 155–1200 days) (Fig 1), whereas 75 nodules were found to have transformed to hypervascular HCC at follow-up MR imaging (group 2) (mean follow-up, 388 days; range, 92–1020 days) (Fig 2). All patients underwent single- or multisession follow-up multidetector CT during the interval between the initial MR examination and the last MR examination. Fifty patients also underwent additional single- or multi-session (two to four) follow-up liver MR imaging during the interval between the initial and the last MR examination. Evidence of hypervascular HCC was not demonstrated, neither at multi–detector row CT nor at interval MR imaging.

MR Examinations

All MR imaging examinations were performed by using a 3.0-T whole-body MR system (Intera Achieva; Philips Healthcare), with a 16-channel phased-array coil used as the receiver coil. The baseline MR imaging included a T1-weighted turbo field-echo in-phase and opposed-phase sequence, a breath-hold multishot T2-weighted sequence, and a respiratory-triggered heavily T2-weighted sequence. DW images were acquired by using a respiratory-triggered single-shot echo-planar imaging with a b value of 0, 100, and 800 sec/mm^2.

For gadoxetic acid–enhanced imaging, unenhanced, arterial phase (20–35 seconds), portal phase (60 seconds), late phase (3 minutes), and 20-minute HBP images were obtained by using a T1-weighted, three-dimensional turbo field-echo sequence (T1-weighted high-resolution isotropic volume examination, THRIVE; Philips Healthcare). The measured voxel size was 1.5 × 1.5 × 4.0 mm, and the reconstructed voxel size was 1.17 × 1.17 × 2.0 mm. The time for the arterial phase imaging was determined by using the MR fluoroscopic bolus detection technique. By using a power injector, the contrast agent was administered intravenously at a rate of 1 mL/sec for a dose of 0.025 mmol per kilogram of body weight, followed by a 20-mL saline flush. We chose an injection rate of 1 mL/sec to reduce ringing (truncation) artifacts observed during the arterial phase, which occur if the contrast agent abruptly flows into the imaging field when the central k-space is filled, disrupting k-space homogeneity (14). The detailed parameters of the MR sequences used are shown in Table 1.

Image Analysis

All MR images were evaluated by two gastrointestinal radiologists (Y.K.K. and M.J.P., with 11 and 6 years of experience in the interpretation of liver MR imaging, respectively) in consensus. All images were evaluated by using a picture archiving and communication system (Pathspeed; GE Medical Systems Integrated Imaging Solutions, Mt Prospect, Ill), with an adjustment of the optimal window setting in each case. The initial MR images of groups 1 and 2 were presented randomly in a blinded manner to avoid bias. The parameters evaluated on the initial MR images included the nodule size, degree of hypointensity on HBP images, presence of fat component, signal intensity on T1-weighted and T2-weighted images, and presence of hyperintensity on high-b-value DW images (b = 800 sec/mm^2). The lesion size was measured as the longest nodule diameter on the 20-minute HBP image. The degree of nodule hypointensity on HBP images was categorized by using a four-point grading system as follows: grade 1, higher than that of the psoas muscle (least hypointense); grade 2, equal to that of the psoas muscle; grade 3, less than that of the psoas muscle but higher than that of the intrahepaic portal vein; and grade 4, equal to or lower than that of the intrahepatic portal vein (most hypointese). The presence of fat component in the nodule was determined on the basis of signal decrease on opposed-phase compared with in-phase T1-weighted images. The signal intensity of the nodule relative to that of the surrounding liver parenchyma on T1- and T2-weighted images, as well as on high-b-value DW images, was classified as follows: hypointense, isointense or invisible, or hyperintense. We measured the apparent diffusion coefficient (ADC) for each nodule at the initial DW imaging. The b values of 0 and 800 sec/mm^2 were used to generate the ADC map.

Statistical Analysis

The clinical characteristics of both groups were compared by using a Mann-Whitney U test for continuous values and a χ^2 test or Fisher exact test for proportions. The baseline characteristics of the hypointense nodules on HBP images that subsequently developed into hypervascular

Figure 1

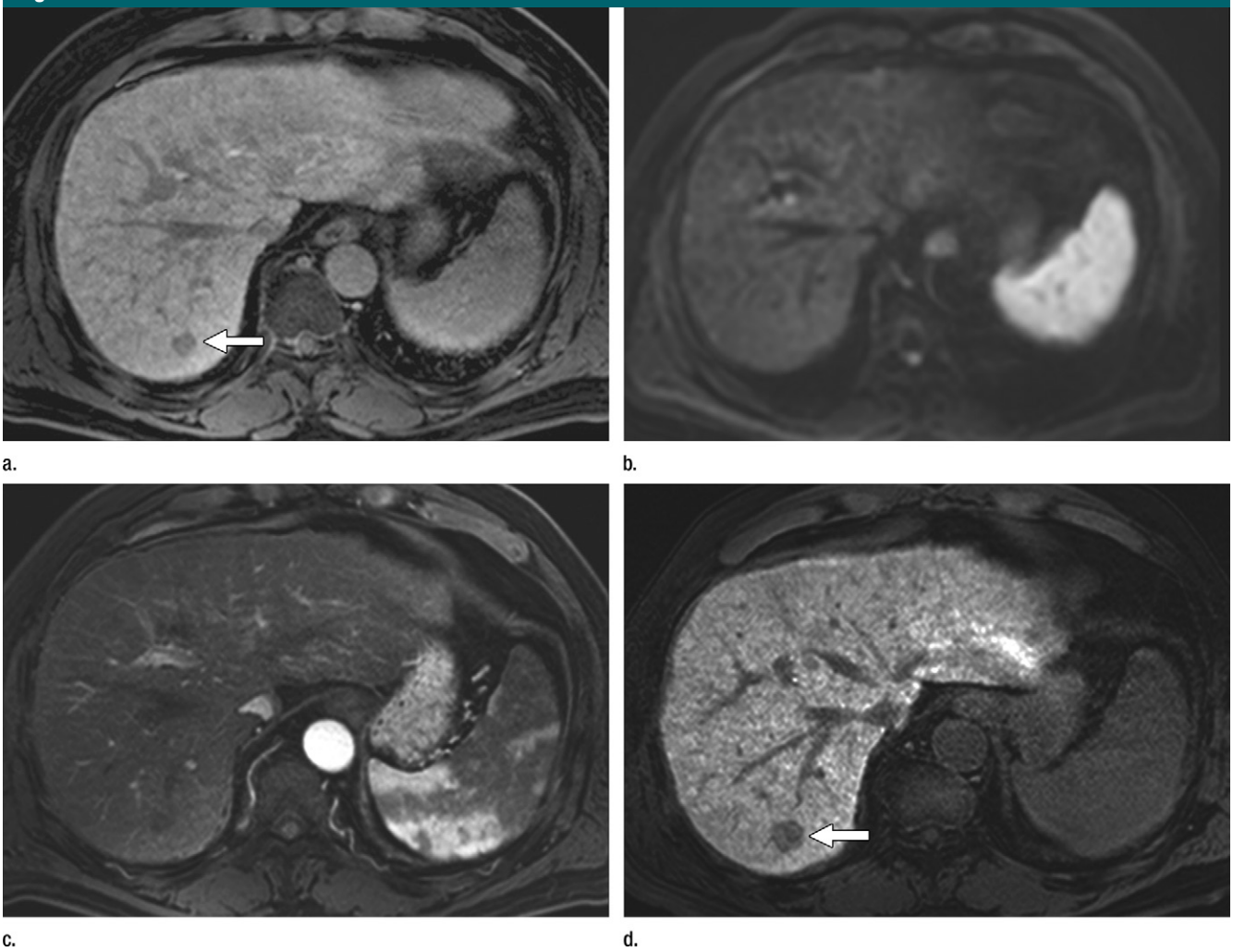

Figure 1: Borderline nodule that did not progress to hypervascular HCC in a 61-year-old man with hepatitis B–induced liver cirrhosis. **(a)** Axial gadoxetic acid–enhanced 20-minute HBP image shows a hypointense nodule (arrow). **(b)** Axial single-shot echo-planar DW image (b = 800 sec/mm^2) shows no liver mass. **(c, d)** Axial gadoxetic acid–enhanced MR images obtained 16 months later show no enhancing mass lesion at **(c)** arterial phase and a hypointense nodule (arrow) with an interval increase in size, compared with that on **a,** at **(d)** 20-minute HBP.

HCCs and those that did not were compared on the initial MR images. The patients' history of HCC was also considered as a variable. Hypervascular HCC-free survival time was calculated from the date of acquisition of the initial MR images to the date of acquisition of the final follow-up MR images or development of hypervascular HCC. Univariable Cox regression analysis of the clustered data was used to test for the association between the baseline characteristics and the development of hypervascular HCC. Multivariable analysis conducted by using a Cox proportional hazards model for the clustered data was performed to identify predictive variables while adjusting for the other characteristics. All variables were included in a full model, and the parameter estimates for this full model are provided. Hazard ratios and the corresponding 95% confidence intervals (CIs) were reported. For multilevel categorical variables, 95% CIs for hazard ratios applied by Bonferroni correction were estimated. A two-sided P value of less than .05 was considered to indicate statistically significant difference. Statistical analysis was performed by using SAS version 9.1.3 (SAS Institute, Cary, NC) and R 2.13.2 (R Foundation for Statistical Computing, Vienna, Austria; *www.R-project.org*) software.

Results

Table 2 shows a summary of the demographic and clinical characteristics of each group. Of 135 patients, 57 had

Figure 2

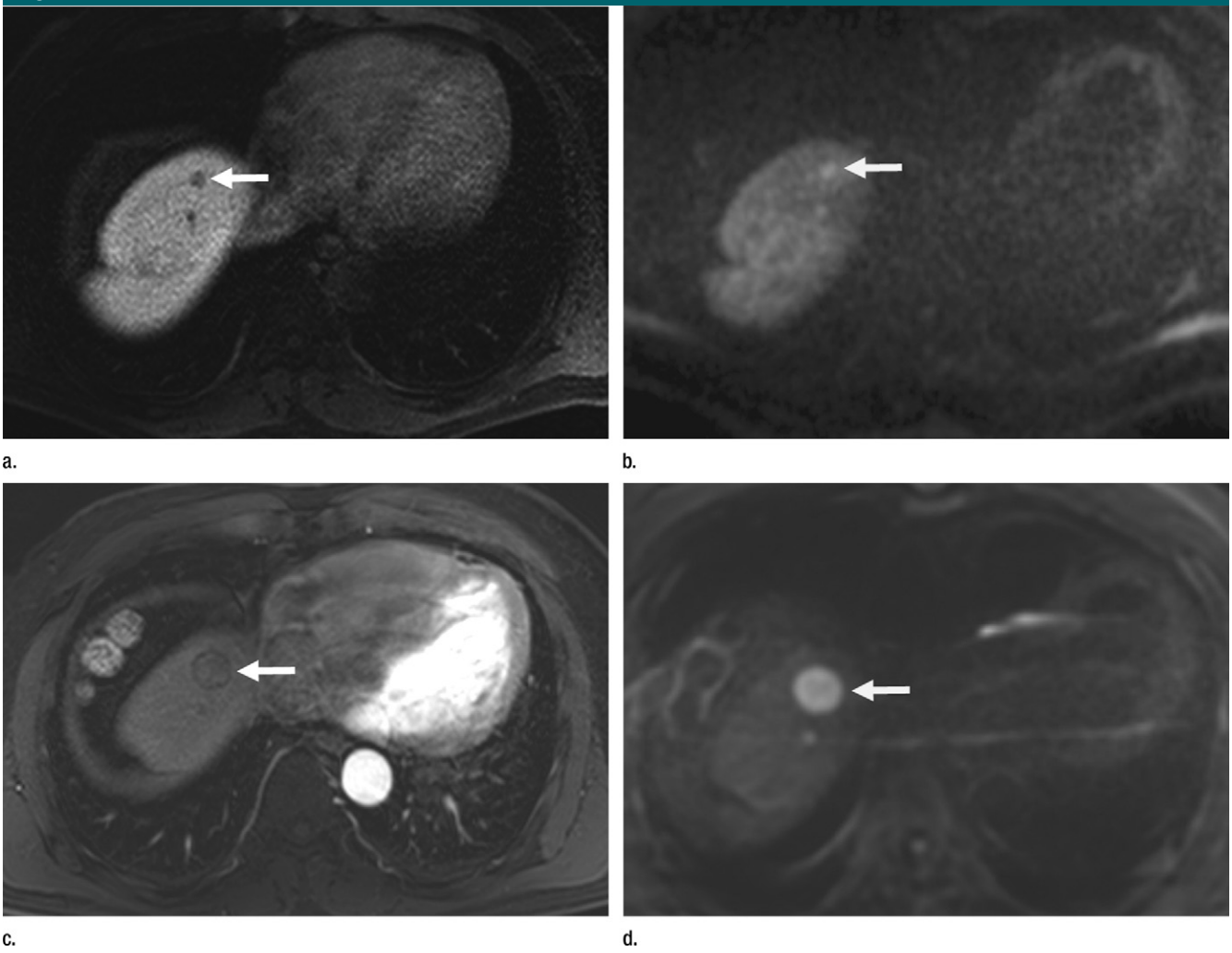

Figure 2: Borderline hepatocellular nodule that progressed to hypervascular HCC in a 62-year-old man with hepatitis B–induced liver cirrhosis. **(a)** Axial gadoxetic acid–enhanced 20-minute HBP image shows a tiny hypointense nodule (arrow) in the hepatic dome. **(b)** Axial single-shot echo-planar DW image (b = 800 sec/mm^2) shows a bright hyperintense lesion in the same location (arrow). **(c)** Axial gadoxetic acid–enhanced arterial phase image obtained 12 months later shows arterial hypervascularization with an interval increase in size (arrow). **(d)** Axial single-shot echo-planar DW image (b = 800 sec/mm^2) obtained 12 months later shows a bright hyperintense lesion in the same location (arrow).

75 hypointense nodules on HBP images that transformed into hypervascular HCC (Fig 2). Forty-two patients had one solitary lesion, 12 had two lesions, and three had three lesions. Of 214 hypointense nodules on HBP images, seven nodules in seven patients proved to be high-grade (n = 3) or low-grade (n = 4) dysplastic nodules at liver biopsy performed after initial MR examination. On initial DW images, one high-grade dysplastic nodule was hyperintense and transformed into hypervascular HCC (group 2) and the others were isointense. The diagnosis of 75 hypervascular HCCs (group 2) was confirmed on the basis of surgical specimens in 10 patients and at core-needle biopsy in two patients. In the remaining 45 patients who underwent transarterial chemoembolization (n = 35) or radiofrequency ablation (n = 10), all tumors fitted into the criteria for the diagnosis of HCC as recommended by the American Association for the Study of Liver Diseases (15), because they showed arterial hypervascularization and early wash-out (with hypointensity at HBP) at both multidetector CT and MR imaging. All but one of the 75 HCCs showed hyperintensity on DW- and T2-weighted images. Five lesions demonstrated a nodule in nodule appearance, that is, hypovascular borderline nodule containing a distinct subnodule with typical features of advanced HCC

Table 1

MR Imaging Sequences and Parameters

Sequence	TR (msec)/TE (msec)	Flip Angle (degree)	Section Thickness (mm)	Matrix Size	Bandwidth (Hz/pixel)	Field of View (cm)	Acquisition Time (sec)	No. of Signals Acquired
T1-weighted 2D dual gradient echo	3.5/1.15–2.3	10	6	256 × 194	1918.6/0.226	32–38	14	1
Breath-hold multishot T2 weighted	1623/70	90	5	324 × 235	255.3/1.702	32–38	55	1
Respiratory-triggered single-shot heavily T2 weighted	1156/160	90	5	376 × 270	388.9/1.117	32–38	120	2
T1-weighted 3D gradient echo	3.1/1.5	10	2	256 × 256	723.4/0.601	32–38	16.6	1
DW	1600/70	90	5	112 × 112	79.5/5.467	32–38	126	2

Note.—TR = repetition time, TE = echo time, 2D = two-dimensional, 3D = three-dimensional.

Table 2

Clinical Characteristics of the Two Groups of Patients

Characteristic	Group 1	Group 2	*P* Value
Age (y)*	61.1 ± 9.0	60.2 ± 8.7	.780
Sex			.858
Male	55 (70.5)	41 (71.9)	
Female	23 (29.5)	16 (28.1)	
Child-Pugh class			.753
A	76 (97.4)	56 (98.2)	
B	2 (2.6)	1 (1.8)	
No. of nodules			.055
1	45 (57.7)	42 (73.7)	
>1	33 (42.3)	15 (26.3)	
HCC history			.712
Yes	70 (89.7)	50 (87.7)	
No	8 (10.3)	7 (12.3)	

Note.—Group 1includes 78 patients with 139 stable nodules and group 2 includes 57 patients with 75 nodules that transformed to hypervascular HCC. Data in parentheses are percentages.

* Data are means ± standard deviation.

(arterial hyperenhancement plus early wash-out and hypointensity at HBP) (Fig 3). Of 139 nodules in group 1, two nodules in two patients proved to be a high-grade nodule and a low-grade dysplastic nodule at liver transplantation. A high-grade dysplastic nodule demonstrated hyperintensity on initial DW images.

MR features of both groups for each variable are summarized in Table 3. Univariable Cox analysis revealed that hypointensity at HBP (grade 3 or 4) (P = .044 and 0.001) and hyperintensity at T2-weighted and DW imaging were associated with the development of HCC (P = .001 and .0001, respectively) (Table 4). However, according to the multivariable Cox analysis (Table 5), no other variable significantly adjusted the model once hyperintensity at initial DW imaging was already included as a variable associated with the development of HCC. Thus, hyperintensity at initial DW imaging was the only significant variable associated with the subsequent nodule progression to hypervascular HCC (Figs 2, 3). This feature was found in 42 hypointense nodules in group 2 and in four hypointense nodules in group 1 (P = .0001). The hazard ratio was 7.44 (95% CI: 4.28, 12.94) for hyperintensity at initial DW imaging. Three hypointense nodules depicted at initial HBP imaging showed hyperintensity on DW images, between MR imaging of the initial and the last examination, and then subsequently transformed into hypervascular HCC at the last MR examination. Thus, these three lesions were categorized into group 2 (Fig 4). Eight nodules that were hyperintense on initial T2weighted images also demonstrated hyperintensity on the initial DW images. The history of HCC was not significantly related to the development of HCC (P = .846). The mean ADC of the transformed group at initial MR imaging was significantly lower than that in the stable group (1.14 ± 0.12 vs 1.26 ± 0.14; P = .0001).

Discussion

Hepatocarcinogenesis is a multifactorial process that includes changes in architecture, cellular density, hepatocyte function, and Kupffer cell numbers or function (16). Accordingly, combining gadoxetic acid and DW imaging has the potential to be robust liver MR protocol

Figure 3

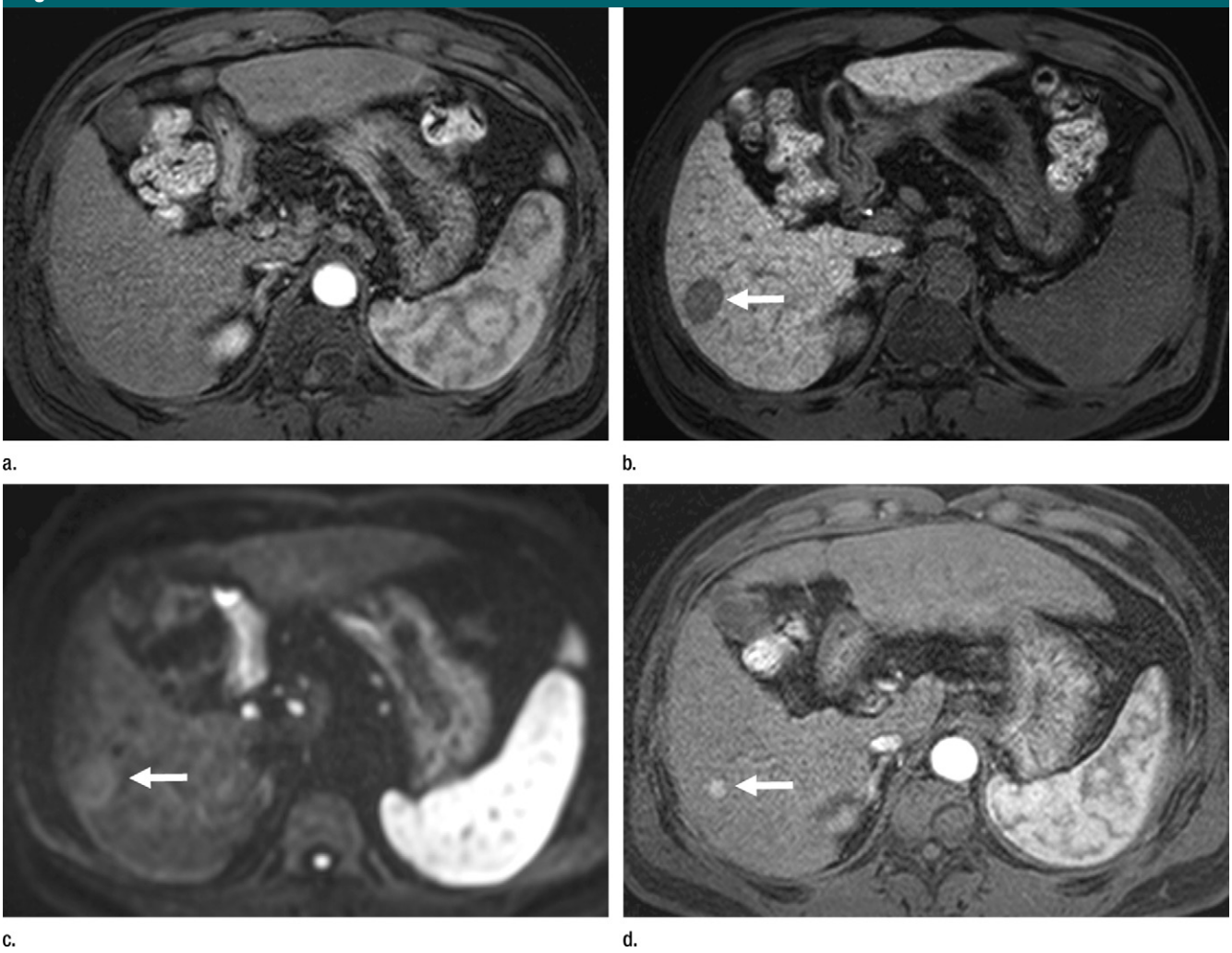

Figure 3: Borderline hepatocellular nodule that progressed to hypervascular HCC in a 59-year-old man with hepatitis B–induced liver cirrhosis. **(a)** Axial gadoxetic acid–enhanced arterial phase image shows no enhancing mass. **(b)** Axial gadoxetic acid–enhanced 20-minute HBP image shows a hypointense nodule (arrow). **(c)** Axial single-shot echo-planar DW image (b = 800 sec/mm^2) shows subtle hyperintensity (arrow) in the same location as **b**. **(d)** Axial gadoxetic acid–enhanced arterial phase image obtained 15 months later shows a small hyperenhancing area (arrow) in the same location as **b**, representing "nodule in nodule appearance."

in that it is targeting three processes of hepatic carcinogenesis: hemodynamic changes, hepatocyte function, and tissue diffusivity (17–19). Although the differentiation of solid liver tumors such as HCC, focal nodular hyperplasia, and adenoma may be difficult with DW imaging alone, the presence of a solid mass in a cirrhotic liver with restricted diffusion may be confirmatory for HCC when other MR features of HCC are present (17–19).

Our results indicated that hyperintensity on DW images is the only independent predictive imaging feature of hypointense nodules at HBP to transform into hypervascular HCC. This feature was found in 42 nodules in group 2 and in four nodules in group 1 (P = .0001). In addition, in line with the findings of previous reports (17–19), most hypervascular HCCs verified at the last MR examination in our study (74 of 75) showed hyperintensity on the last follow-up DW images. In view of this, we questioned whether hypointense nodules at HBP showing DW hyperintensity were already HCC. However, among hypointense nodules at HBP showing DW hyperintensity, two lesions proved to be high-grade dysplastic nodules at histologic examination. This is also true for one lesion that we excluded from this study as well. Thus, our study indicated that diffusion restriction might not necessarily reflect HCC in the multistep hepatocarcinogenetic pathway. This finding reaffirms the result of a recent report (20), which demonstrated three benign hepatocellular nodules showing hyperintensity on DW images. However, as was shown in six HCCs ultimately not included in this study, hypovascular HCC can also be seen in hypointense nodules

Table 3

Characteristics of Hypovascular Hypointense Nodules on HBP Gadoxetic Acid–enhanced MR Images with and without Risk for Developing into Hypervascular HCC

Characteristic	Group 1 ($n = 139$)	Group 2 ($n = 75$)
Degree of hypointensity at HBP		
1	8 (6.0)	3 (4.4)
2	53 (39.6)	9 (13.0)
3	49 (36.6)	30 (43.5)
4	24 (17.9)	27 (39.1)
Initial lesion size (mm)*	11.5 ± 4.7	11.0 ± 6.1
Fat component	8 (5.8)	3 (4.0)
T1-weighted imaging		
Isointense	115 (85.8)	63 (84.0)
Hyperintense	19 (14.2)	12 (16.0)
T2-weighted imaging		
Hypointense	17 (12.2)	4 (5.3)
Isointense	121 (87.1)	64 (85.3)
Hyperintense	1 (0.7)	7 (12.3)
DW imaging		
Isointense	135 (97.1)	33 (44.0)
Hyperintense	4 (2.9)	42 (56.0)
History of HCC	128 (92.1)	65 (86.7)

Note.—Group1 includes hypovascular hypointense nodules that did not develop into HCC, and group 2 includes hypovascular hypointense nodules that progressed to HCC.

* Data are means ± standard deviation.

at HBP, which were hyperintense on DW images.

Precise histopathologic differentiation between dysplastic nodules and early HCC is still difficult (12); thus, we accept that it is difficult to determine the exact stage of hepatocellular nodules in the gray area of hepatocarcinogenesis, even with use of MR imaging with multiparametric data. We could not reach any conclusion regarding appropriate image guidelines for confidently distinguishing between dysplastic nodules and hypovascular HCC. However, to date, an imaging diagnosis of HCC is achieved only for nodules larger than 1 cm in diameter and showing typical vascular pattern (15).

It needs to be emphasized that three hypointense nodules observed on the initial HBP images first showed hyperintensity on DW images acquired between the initial and last MR examination and then subsequently transformed into hypervascular HCC on the last MR examination. Therefore, it may be a reasonable assumption that HBP-hypointense nodules that subsequently develop HCC might be high-grade dysplastic nodules or early HCC immediately before the stage of hypervascular advanced HCC (1–4). This notion could be supported by five hypointense nodules on HBP images that showed hyperintensity on DW images and transformed into a nodule in nodule appearance during follow-up, indicating a distinct focus of advanced HCC within hypovascular high-grade dysplastic nodule or early HCC (Fig 4) (21). Given that one of the major histologic differences between dysplastic nodule and early HCC is the degree of cellular density (2), DW imaging might be more sensitive in depicting histologic changes of borderline hepatocellular nodules than is liver imaging using an extracellular-space contrast agent. However, in consideration of de novo hepatocarcinogenesis, we acknowledge that all borderline hepatocellular nodules may not show the aforementioned sequential signal intensity changes during hepatocarcinogenesis. Our results raise the question whether DW imaging has the potential to establish the imaging categorization of borderline hepatocellular nodules, which might be distinct from the histopathologic categorization or can be used as a biomarker of the transition from hypovascular borderline hepatocellular nodules to hypervascular HCCs.

Since the background cirrhotic liver also shows restricted diffusion, it might be more difficult to identify hepatocellular nodules showing diffusion restriction in the background cirrhotic liver than in the normal liver (22). Further, when compared with metastases, HCCs are less cellular and therefore not reliably detectable with DW imaging (17,18). Nevertheless, all but one of the 75 HCCs (98.7%) showed hyperintensity on DW images in our study. This value is higher than those of previous reports with use of 1.5-T MR imager (17,18, 19), in which hyperintensity of HCC on DW images was demonstrated (ie, 91.2% [114 of 125], 61.1% [11 of 18], 72% [79 of 109], and 82% [89 of 109]). The interpretation of high frequency of HCCs, as well as borderline hepatocellular nodules, being hyperintense on DW images should take the acquisition technique for DW imaging used in our study into consideration. The main advantage derived from using high-field-strength 3.0-T MR imaging is that it offers theoretical enhanced signal-to-noise ratio and lesion-to-liver contrast when compared with 1.5-T MR imaging. We also applied a parallel acquisition technique with a factor of four. This allowed us to reduce the echo train length by decreasing phase-encoding steps in combination with the faster k-space traversal per unit of time, thereby leading to decreased susceptibility and chemical shift artifacts by not introducing the latter half of the echo train, which is much responsible for those artifacts (23). In addition, multiple-signal acquisition would have increased the possibility of acquiring data during the diastolic phase, which could reduce the subcardiac signal attenuation due to cardiac motion during the systolic phase (23).

Table 4

Univariate Analysis by Using Cox Proportional Hazards Model for Hypovascular Hypointense Nodules on HBP Gadoxetic Acid–enhanced MR Images to Transform into Hypervascular HCC

Nodule Characteristic	Coefficient	Robust SE	Wald Score	*P* Value	Hazard Ratio	95% CI
Degree of hypointensity at HBP						
1	0.526	0.602	0.873	.348	1.692	0.400, 7.157
3	1.001	0.409	2.443	.044	2.719	1.020, 7.247
4	1.379	0.379	3.633	.001	3.973	1.601, 9.863
Lesion size	−0.031	0.036	−0.848	.398	0.969	0.903, 1.041
Fat component	−0.517	0.558	−0.927	.354	0.596	0.199, 1.779
T1-weighted images	0.126	0.420	0.299	.764	1.134	0.498, 2.584
T2-weighted images						
Isointense	−1.718	0.362	−4.749	.001	0.179	0.079, 0.404
Hypointense	−2.223	0.613	−3.628	.001	0.108	0.027, 0.427
DW images	2.119	0.265	7.968	.0001	8.323	4.942, 14.016
HCC history	−0.108	0.558	−0.194	.846	0.897	0.300, 2.684

Note.—*P* value and 95% CI for hazard ratio were corrected by means of Bonferroni method. SE = standard error.

Table 5

Multivariate Analysis by Using Cox Proportional Hazards Model for Hypovascular Hypointense Nodules on HBP Gadoxetic Acid–enhanced MR Images to Transform into Hypervascular HCC

Nodule Characteristic	Coefficient	Robust SE	Wald Score	*P* Value	Hazard Ratio	95% CI
Degree of hypointensity at HBP						
1	−0.087	0.792	−0.110	>.99	0.916	0.138, 6.095
3	0.689	0.394	1.749	.241	1.993	0.776, 5.118
4	1.032	0.383	2.698	.166	2.329	0.813, 6.645
Lesion size	−0.003	0.023	−0.138	.890	0.997	0.954, 1.042
Fat component	−0.954	0.475	−2.006	.145	0.385	0.152, 0.978
T1-weighted images	0.634	0.391	1.620	.105	1.884	0.876, 4.056
T2-weighted images	−0.699	0.413	−1.694	.181	0.497	0.197, 1.254
Isointense						
Hypointense	−0.639	0.798	−0.801	.846	0.528	0.088, 3.158
DW images	2.007	0.282	7.116	.0001	7.444	4.283, 12.941
HCC history	−0.209	0.584	−0.357	.721	0.812	0.258, 2.550

Note.—*P* value and 95% CI for hazard ratio were corrected by means of Bonferroni method. SE = standard error.

Our study had several limitations. First, the majority of lesions were not surgically confirmed. Thus, we could not determine the exact stage of borderline hypointense nodules in the stepwise hepatocarcinogenetic pathway. Second, owing to the retrospective study design, the follow-up interval and follow-up duration were not consistent among the study patients. Thus, an appropriate follow-up period for early recognition of the development of HCC or the cumulative incidence of HCC in the high-risk group could not be determined in this study. Third, the selection bias may have affected our results because our policy is that liver MR imaging is conducted in patients suspected of having HCC based on multidetector CT findings. Thus, most hypointense nodules observed at HBP were detected in patients who previously underwent curative treatment of HCC or in those with coexisting HCCs. This might affect our study result that showed no significant difference in the prevalence of HCC history between the two groups. Nevertheless, it is also highly relevant to recognize the borderline nodules at high risk for progression to hypervascular HCC in patients with HCCs in order to perform tumor staging and determine the therapeutic plan. Future studies need to include patients who do not have a diagnosis of HCC who can be studied prospectively to determine whether or not all hypointense nodules on HBP images would show hyperintensity on DW images before progressing to hypervascular HCC.

Figure 4

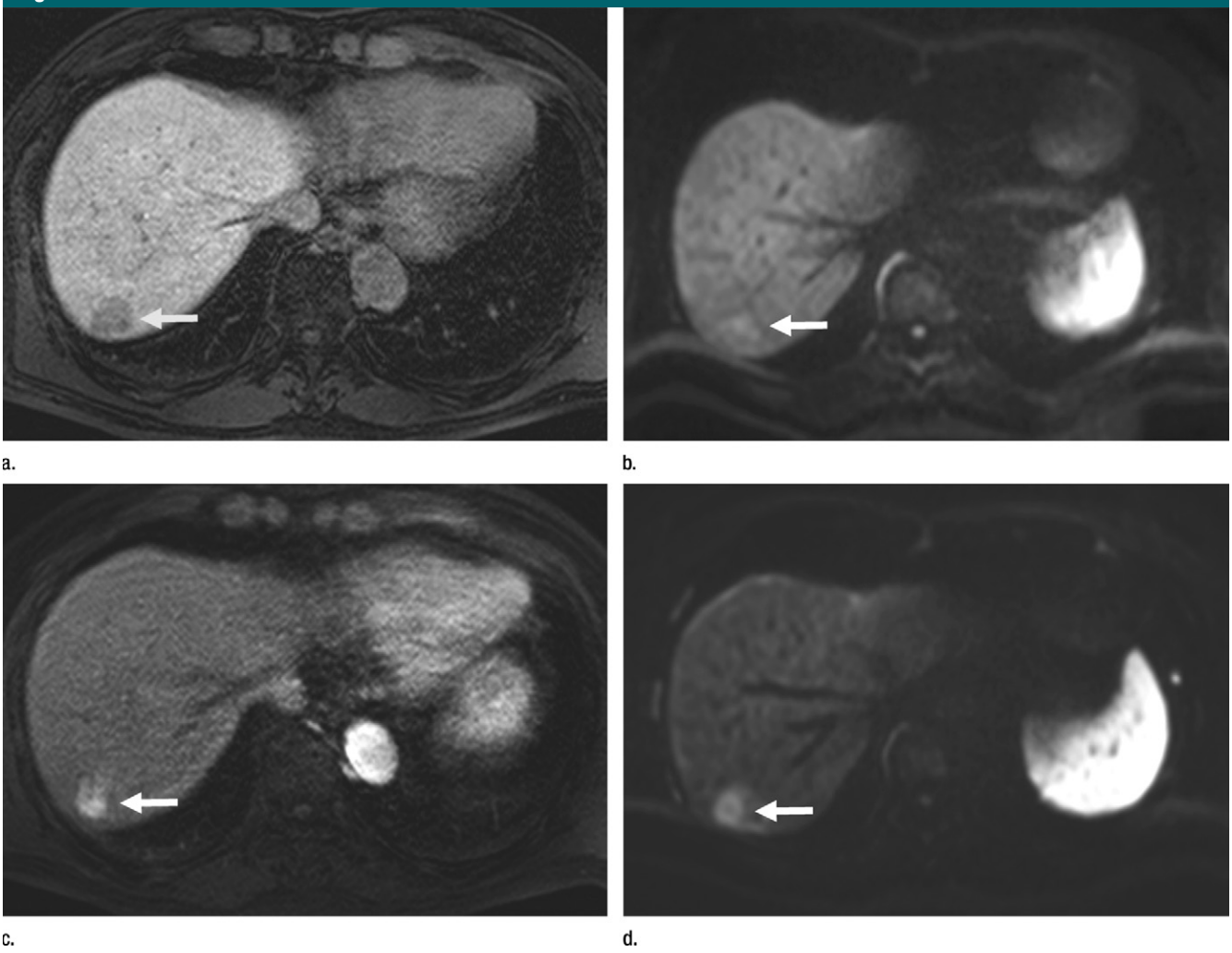

Figure 4: Borderline hepatocellular nodule that progressed to hypervascular HCC in a 68-year-old man with hepatitis B–induced liver cirrhosis. **(a)** Axial gadoxetic acid–enhanced 20-minute HBP image shows a hypointense nodule (arrow). **(b)** Axial single-shot echo-planar DW image ($b = 800$ sec/mm^2) obtained 9 months later shows subtle hyperintensity (arrow) in the same location as **a**. **(c)** Axial gadoxetic acid–enhanced arterial phase image obtained 12 months later shows a hyperenhancing lesion (arrow) in the same location as **a**. **(d)** Axial single-shot echo-planar DW image ($b = 800$ sec/mm^2) obtained 12 months later shows a hyperintense nodule (arrow) in the same location as **c**.

In conclusion, hyperintensity on DW images was strongly associated with progression of hypovascular hypointense nodules at HBP of gadoxetic acid-enhanced MR imaging to hypervascular HCC in patients with hepatitis B–induced liver cirrhosis. Therefore, when we encounter hypointense nodules on HBP gadoxetic acid–enhanced MR images with accompanying hyperintensity on DW images, more careful follow-up or aggressive diagnostic procedures should be considered.

Disclosures of Potential Conflicts of Interest: Y.K.K. No potential conflicts of interest to disclose. **W.J.L.** No potential conflicts of interest to disclose. **M.J.P.** No potential conflicts of interest to disclose. **S.H.K.** No potential conflicts of interest to disclose. **H.R.** No potential conflicts of interest to disclose. **D.C.** No potential conflicts of interest to disclose.

References

1. Sakamoto M, Hirohashi S, Shimosato Y. Early stages of multistep hepatocarcinogenesis: adenomatous hyperplasia and early hepatocellular carcinoma. Hum Pathol 1991;22(2):172–178.
2. Takayama T, Makuuchi M, Hirohashi S, et al. Malignant transformation of adenomatous hyperplasia to hepatocellular carcinoma. Lancet 1990;336(8724):1150–1153.
3. Kudo M. Multistep human hepatocarcinogenesis: correlation of imaging with pathology. J Gastroenterol 2009;44(Suppl 19):112–118.
4. Kitao A, Zen Y, Matsui O, Gabata T, Nakanuma Y. Hepatocarcinogenesis: multistep changes of drainage vessels at CT during arterial portography and hepatic arteriography—radiologic-pathologic correlation. Radiology 2009;252(2):605–614.

5. Di Martino M, Marin D, Guerrisi A, et al. Intraindividual comparison of gadoxetate disodium-enhanced MR imaging and 64-section multidetector CT in the detection of hepatocellular carcinoma in patients with cirrhosis. Radiology 2010;256(3):806–816.
6. Huppertz A, Haraida S, Kraus A, et al. Enhancement of focal liver lesions at gadoxetic acid-enhanced MR imaging: correlation with histopathologic findings and spiral CT—initial observations. Radiology 2005;234(2):468–478.
7. Kim YK, Kim CS, Han YM, Park G. Detection of small hepatocellular carcinoma: can gadoxetic acid-enhanced magnetic resonance imaging replace combining gadopentetate dimeglumine-enhanced and superparamagnetic iron oxide-enhanced magnetic resonance imaging? Invest Radiol 2010;45(11):740–746.
8. Ahn SS, Kim MJ, Lim JS, Hong HS, Chung YE, Choi JY. Added value of gadoxetic acid-enhanced hepatobiliary phase MR imaging in the diagnosis of hepatocellular carcinoma. Radiology 2010;255(2):459–466.
9. Motosugi U, Ichikawa T, Sou H, et al. Distinguishing hypervascular pseudolesions of the liver from hypervascular hepatocellular carcinomas with gadoxetic acid-enhanced MR imaging. Radiology 2010;256(1):151–158.
10. Park G, Kim YK, Kim CS, Yu HC, Hwang SB. Diagnostic efficacy of gadoxetic acid-enhanced MRI in the detection of hepatocellular carcinomas: comparison with gadopentetate dimeglumine. Br J Radiol 2010;83(996):1010–1016.
11. Kim MJ. Current limitations and potential breakthroughs for the early diagnosis of hepatocellular carcinoma. Gut Liver 2011;5(1):15–21.
12. Kojiro M. Diagnostic discrepancy of early hepatocellular carcinoma between Japan and West. Hepatol Res 2007;37(Suppl 2):S121–S124.
13. Hayashi M, Matsui O, Ueda K, Kawamori Y, Gabata T, Kadoya M. Progression to hypervascular hepatocellular carcinoma: correlation with intranodular blood supply evaluated with CT during intraarterial injection of contrast material. Radiology 2002;225(1):143–149.
14. Tanimoto A, Lee JM, Murakami T, Huppertz A, Kudo M, Grazioli L. Consensus report of the 2nd International Forum for Liver MRI. Eur Radiol 2009;19(Suppl 5):S975–S989.
15. Bruix J, Sherman M; American Association for the Study of Liver Diseases. Management of hepatocellular carcinoma: an update. Hepatology 2011;53(3):1020–1022.
16. Kojiro M. Pathology of hepatocellular carcinoma. Oxford, England: Blackwell, 2006; 1–7.
17. Nasu K, Kuroki Y, Tsukamoto T, Nakajima H, Mori K, Minami M. Diffusion-weighted imaging of surgically resected hepatocellular carcinoma: imaging characteristics and relationship among signal intensity, apparent diffusion coefficient, and histopathologic grade. AJR Am J Roentgenol 2009;193(2):438–444.
18. Kim YK, Kim CS, Han YM, Lee YH. Detection of liver malignancy with gadoxetic acid-enhanced MRI: is addition of diffusion-weighted MRI beneficial? Clin Radiol 2011;66(6):489–496.
19. Piana G, Trinquart L, Meskine N, Barrau V, Beers BV, Vilgrain V. New MR imaging criteria with a diffusion-weighted sequence for the diagnosis of hepatocellular carcinoma in chronic liver diseases. J Hepatol 2011;55(1):126–132.
20. Lee MH, Kim SH, Park MJ, Park CK, Rhim H. Gadoxetic acid-enhanced hepatobiliary phase MRI and high-b-value diffusion-weighted imaging to distinguish well-differentiated hepatocellular carcinomas from benign nodules in patients with chronic liver disease. AJR Am J Roentgenol 2011;197(5):W868–W875.
21. Oikawa T, Ojima H, Yamasaki S, Takayama T, Hirohashi S, Sakamoto M. Multistep and multicentric development of hepatocellular carcinoma: histological analysis of 980 resected nodules. J Hepatol 2005;42(21):225–229.
22. Sandrasegaran K, Akisik FM, Lin C, et al. Value of diffusion-weighted MRI for assessing liver fibrosis and cirrhosis. AJR Am J Roentgenol 2009;193(6):1556–1560.
23. Nasu K, Kuroki Y, Nawano S, et al. Hepatic metastases: diffusion-weighted sensitivity-encoding versus SPIO-enhanced MR imaging. Radiology 2006;239(1):122–130.